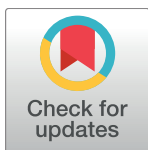


## RESEARCH ARTICLE

# Imidazoquinoxaline anticancer derivatives and imiquimod interact with tubulin: Characterization of molecular microtubule inhibiting mechanisms in correlation with cytotoxicity



Alexis Courbet<sup>1,2\*</sup>, Nicole Bec<sup>1,3,4,5</sup>, Caroline Constant<sup>4</sup>, Christian Larroque<sup>1,3,4,5</sup>, Martine Pugnieri<sup>1,3,4,5</sup>, Safia El Messaoudi<sup>1,3,4,5</sup>, Zahraa Zghaib<sup>6</sup>, Sonia Khier<sup>1,3,4,5</sup>, Carine Deleuze-Masquefa<sup>6</sup>, Florence Gattaccea<sup>1,3,4,5\*</sup>

**1** University of Montpellier, Montpellier, France, **2** Department of Biochemistry & Institute for Protein Design, University of Washington, Seattle, WA, United States of America, **3** IRCM, Institut de Recherche en Cancérologie de Montpellier, Montpellier, France, **4** IRCM, Institut de Recherche en Cancérologie de Montpellier INSERM U1194, Montpellier, France, **5** Institut Régional du Cancer de Montpellier, Montpellier, France, **6** IBMM, Institut des Biomolécules Max Mousseron, UMR 5247, Université de Montpellier, Montpellier, France

\* [acourbet@uw.edu](mailto:acourbet@uw.edu) (AC); [florence.gattaccea@umontpellier.fr](mailto:florence.gattaccea@umontpellier.fr) (FG)

## OPEN ACCESS

**Citation:** Courbet A, Bec N, Constant C, Larroque C, Pugnieri M, El Messaoudi S, et al. (2017) Imidazoquinoxaline anticancer derivatives and imiquimod interact with tubulin: Characterization of molecular microtubule inhibiting mechanisms in correlation with cytotoxicity. PLoS ONE 12(8): e0182022. <https://doi.org/10.1371/journal.pone.0182022>

**Editor:** Salvatore V Pizzo, Duke University School of Medicine, UNITED STATES

**Received:** December 5, 2016

**Accepted:** July 11, 2017

**Published:** August 10, 2017

**Copyright:** © 2017 Courbet et al. This is an open access article distributed under the terms of the [Creative Commons Attribution License](#), which permits unrestricted use, distribution, and reproduction in any medium, provided the original author and source are credited.

**Data Availability Statement:** All relevant data are within the paper and its Supporting Information files.

**Funding:** This work was supported by a grant from GEFLUC Montpellier (Groupements des Entreprises Françaises dans la Lutte contre le Cancer) and by the Elie Bzoura grant from SFPO (Société Française de Pharmacie Oncologique) and ANP (Académie Nationale de Pharmacie), Palmarès 2011. The

## Abstract

Displaying a strong antiproliferative activity on a wide variety of cancer cells, EAPB0203 and EAPB0503 belong to the imidazo[1,2-*a*]quinoxalines family of imiquimod structural analogues. EAPB0503 has been shown to inhibit tubulin polymerization. The aim of the present study is to characterize the interaction of EAPB0203 and EAPB0503 with tubulin. We combine experimental approaches at the cellular and the molecular level both *in vitro* and *in silico* in order to evaluate the interaction of EAPB0203 and EAPB0503 with tubulin. We examine the influence of EAPB0203 and EAPB0503 on the cell cycle and fate, explore the binding interaction with purified tubulin, and use a computational molecular docking model to determine the binding modes to the microtubule. We then use a drug combination study with other anti-microtubule agents to compare the binding site of EAPB0203 and EAPB0503 to known potent tubulin inhibitors. We demonstrate that EAPB0203 and EAPB0503 are capable of blocking human melanoma cells in G2 and M phases and inducing cell death and apoptosis. Second, we show that EAPB0203 and EAPB0503, but also unexpectedly imiquimod, bind directly to purified tubulin and inhibit tubulin polymerization. As suggested by molecular docking and binding competition studies, we identify the colchicine binding site on  $\beta$ -tubulin as the interaction pocket. Furthermore, we find that EAPB0203, EAPB0503 and imiquimod display antagonistic cytotoxic effect when combined with colchicine, and disrupt tubulin network in human melanoma cells. We conclude that EAPB0203, EAPB0503, as well as imiquimod, interact with tubulin through the colchicine binding site, and that the cytotoxic activity of EAPB0203, EAPB0503 and imiquimod is correlated to their tubulin inhibiting effect. These compounds appear as interesting anticancer drug candidates as suggested by their activity and mechanism of action, and deserve further investigation for their use in the clinic.

funders had no role in study design, data collection and analysis, decision to publish, or preparation of the manuscript.

**Competing interests:** The authors have declared that no competing interests exist.

## Introduction

Imiquimod (Aldara®) is a commercially available drug approved by the US Food and Drug Administration in 1997 to treat actinic keratosis, external genital warts, and superficial basal cell carcinoma [1]. Imiquimod is also under evaluation and/or currently used off-label in various malignancies. Efficacy against melanoma was demonstrated in a mouse model [2]. Used alone, imiquimod was able to clear an invasive melanoma in a 93-year-old woman [3]. In recent clinical trials, imiquimod used in combination was also proved efficient to treat superficial cutaneous melanoma metastases [4–6]. However, imiquimod is approved only as a topical cream, because it induced significant side effects that led to dose reduction or cure stop when given orally to cancer patients in a phase I clinical trial [7]. Even used as a topical treatment, imiquimod induces uncommon systemic side effects [8]. This underlines the usefulness of developing analogues with better efficiency and/or less general toxicity.

A series of heterocyclic compounds, the imidazo[1,2-*a*]quinoxalines family, nick-named *imiquinalines*, was developed from structural analogy with imiquimod and synthesized by C. Deleuze-Masquefa and P.-A. Bonnet group [9,10]. These compounds displayed a direct antiproliferative effect on A375 highly resistant human melanoma cancer cell line, and the compound EAPB0203 (*N*-methyl-1-(2-phenylethyl)imidazo[1,2-*a*]quinoxalin-4-amine) was identified as the initial leader of the series [11] (Fig 1). The 50% inhibitory of maximum concentration ( $IC_{50}$ ) obtained in the A375 model for EAPB0203 was 1.57  $\mu$ M, which was far lower than that obtained with imiquimod (70.3  $\mu$ M) [11]. EAPB0203 was also cytotoxic at  $\mu$ M concentrations in adult T-cell leukemia/lymphoma (ATLL) cell lines and primary cells [12], and in chronic myeloid leukemia (CML) cell lines [13]. Interestingly, while imiquimod induced dose-limiting lymphocytopenia in phase I clinical trials [7,14], EAPB0203 10  $\mu$ M was not cytotoxic toward non-malignant T lymphocytes. EAPB0203 also significantly inhibited tumor growth in nude mice xenografted with M4Be human melanoma cell line, to a greater extent than fotemustine [11], which was the second most commonly used first-line systemic treatment for metastatic melanoma in Europe [15].

Further pharmacomodulation of imiquinalines lead to new compounds [16]. Among them, EAPB0503 (1-(3-methoxyphenyl)-*N*-methylimidazo[1,2-*a*]quinoxalin-4-amine) displayed a roughly ten times stronger cytotoxic activity than EAPB0203 in A375 cells ( $IC_{50}$  = 0.2  $\mu$ M) [16] and in CML cells [13]. These results were confirmed by the NCI-60 DTP Human Tumor Cell Line Screen (<http://dtp.cancer.gov/>), which showed a mean  $GI_{50}$  (50% Growth Inhibitory Concentration) of 1.12  $\mu$ M for EAPB0203 and of 0.490  $\mu$ M for EAPB0503 in the 60 human tumor cell lines tested.

Interestingly, sub-acute toxicity studies in Sprague Dawley rats receiving intravenous EAPB0203 at 5 mg/kg once daily or EAPB0503 at 3 mg/kg for five consecutive days showed no effect on vital organs nor on blood components [17]. Pharmacokinetic properties and metabolism of EAPB0203 and EAPB0503 have been extensively studied. Metabolism occurred through demethylation and hydroxylation reactions involving mainly cytochrome P450 3A [18].

Therefore, understanding the mechanism of action of these promising therapeutic anticancer molecules, displaying strong cytotoxic activity and low toxicity, is an important step to assess their value for further development. Interestingly, TLR 7/8 agonism exerted by imiquimod is considered the main mechanism explaining its anticancer activity on melanoma, via the induction of pro-inflammatory cytokines leading to activation of DC cells/innate immunity and thereby Th1 antitumoral cellular immune response along with the activation of NF-KB [19]. Independently of TLR-7 and TLR-8 pathways, imiquimod has also been shown to be involved in adenosine signaling via receptor-independent adenylyl cyclase inhibition, the activation of NF-KB, and has also been shown to induce apoptosis of tumor cells at higher concentrations through secondary molecular mechanisms that have not been clearly elucidated.

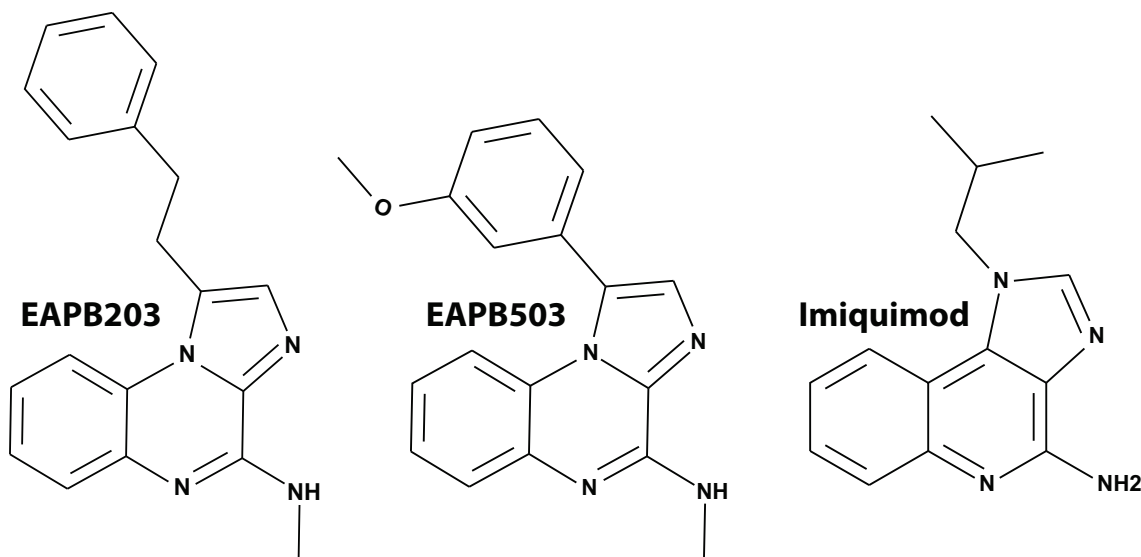


**Fig 1. Chemical structures of studied compounds.** The imidazo[1,2-a]quinoxalines family, nick-named *imiquinalines*, was developed from structural analogy with imiquimod. The compound EAPB0203 (*N*-methyl-1-(2-phenylethyl)imidazo[1,2-a]quinoxalin-4-amine) was identified as the initial leader of the series. Further pharmacomodulation of imiquinalines lead to the new compound EAPB0503 (1-(3-methoxyphenyl)-*N*-methylimidazo[1,2-a]quinoxalin-4-amine).

<https://doi.org/10.1371/journal.pone.0182022.g001>

This pro-apoptotic activity involves caspase activation dependent of Bcl-2 [20]. Interestingly, anti-microtubule agents are now known to induce apoptosis via inhibition of anti-apoptotic Bcl-2 family proteins [21]. Unlike imiquimod which displays pro-inflammatory properties [22], imidazoquinoxalines showed an anti-inflammatory activity [23] associated to TNF-alpha production impairment through activation of p38MAPK pathway and inhibition of PI3K pathway in L929 murine fibroblast cell line. EAPB0203 has been shown to impair cell growth, block cell cycle in G2/M phase, and activate the mitochondrial pathway leading to apoptosis in ATLL cells. EAPB0203 negatively regulated anti-apoptotic proteins like c-IAP-1 and Bcl-XL, induced a loss of mitochondrial membrane potential, cytochrome c cytoplasmic release, and caspases 3 and 9 activation in malignant T cells. EAPB0203 also stabilized the pro-apoptotic proteins p53 and p21 in a dose- and time-dependent manner, activated p38MAPK pathway, and inhibited PI3K pathway [12]. More recently, EAPB0503 and EAPB0203 have been shown to inhibit AR320, K562 and LAMA84 CML cell lines growth. EAPB0503 induced cell cycle arrest in M phase and apoptosis, and down-regulated BCR-ABL protein. Cell growth inhibition was synergistic with imatinib, and imatinib-resistant cells were sensitive to EAPB0503 [13].

The COMPARE analysis [24] of NCI 60 Cell Line screening assay results for EAPB0203 and EAPB0503 *versus* the standards list available at NCI showed high similarity to antimicrotubule agents, particularly maytansine. Based on this information, EAPB0503 and other newly synthesized derivatives of the imidazoquinoxaline family have recently been shown to inhibit tubulin polymerization [25]. The aim of the present study was thus to evaluate EAPB0203 and EAPB0503 interaction with tubulin, in comparison with imiquimod.

## Materials and methods

### Cell culture

Melanoma A375 cell line was kindly provided by the cell culture facility of IRCM (Institut de Recherche en Cancérologie de Montpellier, France). Cell culture products were obtained from

Lonza (Levallois, France). Culture medium was RPMI 1640, supplemented with 10% heat-inactivated (56°C) fetal bovine serum, 1% penicillin-streptomycine 5000 U/mL, and 1% L-glutamine 200 mM. Cells were maintained in a humidified atmosphere of 5% CO<sub>2</sub> at 37°C. Cells were subcultured as to be maintained in the exponentially growing state, cell confluence never exceeding 90%. Trypsin-versene (EDTA) was used to detach the cells, and Dulbecco's Phosphate Buffered Saline (DPBS) for washes.

### Compounds and reactants

EAPB0203 and EAPB0503 were synthesized as previously described [9,13,16]. Compounds and reactants were bought from Sigma-Aldrich (Saint-Quentin Fallavier, France) unless otherwise stated. Imiquimod was obtained from Molekula (Wessex House, Shaftesbury, Dorset, UK). EAPB0203, EAPB0503, imiquimod, colchicine, vinorelbine, nocodazole and warfarin were prepared as 0.1 M stock solutions in dimethyl sulfoxide (DMSO), and stored at -80°C until use. Working solutions of 0.1 or 1 mM were freshly prepared in culture medium for cell experiments, or in appropriate buffer (see below) for purified tubulin experiments. Final concentration of DMSO never exceeded 0.1% in cell culture medium.

### Proliferation kinetics

A375 cells were plated in 6-well plates at 600,000 cells/well density. Cells were treated 24 hours later with two concentrations of EAPB0203 (0.5 and 5 μM) and of EAPB0503 (0.05 and 0.5 μM) bounding their respective IC<sub>50</sub>. Stock solutions were diluted in culture medium to obtain the desired concentrations. Control wells received fresh culture medium alone. Time of treatment was considered time zero. At each time point, supernatant was withdrawn and cells were harvested by trypsinization. Supernatant and cell suspension were diluted together in culture medium, then centrifuged for 5 min at 1400 rpm to remove trypsin. Cells were resuspended in 500 μL DPBS, then counted using CASY Cell Counter (Roche Diagnostics, Meylan, France). In parallel, 100 μL of cell suspension were mixed with 25 μL Trypan Blue solution 0.4% for dead cells staining, and percentage of dead cells was determined by counting at least 200 cells in various fields using a Malassez counting cell. Dead cells were removed from the total cell count to obtain the number of living cells per well.

### Cell cycle: Staining of cells in G2 and M phase

A375 cells plating, treatment and harvest were the same as described for proliferation kinetics, and were performed in parallel. Nocodazole 50 ng/mL was used as a positive control of mitosis phase blockade [26]. Cells were harvested 24 hours after treatment (16 hours for Nocodazole). After centrifugation, cells were washed by dilution in DPBS containing BSA 0.5%, then centrifuged again. Cells were washed twice again in DPBS alone. The final pellet was resuspended in 100 μL DPBS, and 0.9 mL methanol at -20°C was added drop by drop for fixation. The mixture was kept on ice for 30 minutes, then frozen at -20°C. Prior to flow cytometry, 3 mL DPBS-BSA 0.5% were added, and cells centrifuged again. Cell pellet was resuspended in 100 μL DPBS-BSA 0.5%. After a 30 minute-incubation at room temperature, 2 μL of anti-Phospho-Histone H3 (Ser10) (D2C8) XP® Rabbit monoclonal antibody (phycoerythrin conjugate) (anti-PH3) (Cell Signaling Technology, Ozyme, Saint-Quentin en Yvelines, France) were added. A propidium iodide (PI)-RNase solution was prepared by diluting PI solution 1 mg/mL in DPBS to 1.6 μg/mL, and adding 0.1 mg RNase per mL. After 1 hour incubation at room temperature, cells were washed twice with 1 mL DPBS, then resuspended in 500 μL PI-RNase solution. Flow cytometry analysis was performed with FACS Calibur 2 (Plateforme Montpellier RIO Imaging,

France), using two fluorescence channels. Cells in G2/M (stained with PI) and in M (stained with PI and anti-PH3) phases were quantitated using FlowJo software.

### Cell death and apoptosis

A375 cells plating, treatment and harvest were the same as described for proliferation kinetics. Cells were harvested 24, 48 and 72 hours after treatment. Treated cells were double-stained using Annexin V-FITC /7-AAD kit (Beckman Coulter, Villepinte, France), following the provider's procedure. Briefly, binding buffer was diluted to tenth with distilled water and kept on ice. Harvested cells were washed with DPBS-BSA 0.5%, then with DPBS and finally with 1 mL ice-cold DPBS, then centrifuged at 4°C. Cell pellets were resuspended in 200  $\mu$ L 1X binding buffer and kept on ice. 10  $\mu$ L Annexin V-FITC solution and 20  $\mu$ L of 7-AAD Viability Dye were added to 100  $\mu$ L cell suspension. After a 30-minute incubation on ice in the dark, 400  $\mu$ L 1X binding buffer were added. Samples were kept on ice until flow cytometry analysis, within a time period not exceeding 30 minutes. Flow cytometry analysis and quantitation of dead cells (Annexin V and 7-AAD positive) and apoptotic cells (Annexin V positive and 7-AAD negative) were performed as described above for cell cycle.

### Tubulin binding evaluation by Surface Plasmon Resonance (SPR)

Tubulin was prepared from pig brain according to the purification procedure described by Williams and Lee [27]. Surface Plasmon Resonance (SPR) technology was used to evaluate binding to purified tubulin. All analyses were performed on T200 apparatus (GE Healthcare, Montpellier, France) at 25°C. Purified tubulin was covalently immobilized on a CM5 flow cell sensor chip (GE Healthcare) by EDC/NHS (N-(3-dimethylaminopropyl)-N'-ethylcarbodiimide hydrochloride / N-hydroxysuccinimide) activation according to the manufacturer's instructions. Reference flow cells were prepared with the same activation procedure, but without protein or with an irrelevant protein (Anti-GST antibody). EAPB0203, EAPB0503 and imiquimod were injected at different concentrations in HBS-EP+ buffer adjusted at 3% DMSO at a flow rate of 30  $\mu$ L/min on the different flow cells. Concentrations tested were limited by aggregation phenomenon, which occurred for EAPB0203 above 25  $\mu$ M, as determined by dynamic light scattering, with an increased particle size and a polydispersity index superior to 0.7 (S1 Fig). No aggregation was observed for colchicine at 200  $\mu$ M. The binding values were collected after subtraction of the reference flow cell response and solvent correction. Each experiment series included blanks (running buffer), colchicine and warfarin as positive and negative control respectively. The standard error was calculated from four different experiments.

### Polymerization of purified tubulin *in vitro*

Tubulin was prepared from pig brain according to the purification procedure described by Williams and Lee [27]. Tubulin polymerization was monitored turbidimetrically at 350 nm with a MC2 spectrophotometer (Safas, Monaco) equipped with a thermal-jacketed cuvette holder. The reaction mixture was prepared at 0°C, and contained PEM buffer, 25% glycerol (v/v), 1 mM Guanosine Tri Phosphate (GTP), and 2.4  $\mu$ M tubulin. GTP and tubulin were added at the very last minute. EAPB0203, EAPB0503, imiquimod and colchicine stock solutions were diluted in DMSO to the desired concentration, and 1  $\mu$ L of the compound solution was added to the reaction medium. The same volume of DMSO alone was used for negative control. For testing of high concentrations of imiquimod, and for warfarin used as negative control, 20  $\mu$ L of diluted imiquimod, warfarin or of DMSO alone had to be added. The final volume of the sample was 200  $\mu$ L. The reaction was started by placing the cuvette in the

spectrophotometer cell compartment thermostated at 37°C. Ice was added 45 minutes later to initiate depolymerization to check for signal specificity.

Kinetics of purified tubulin assembly *in vitro* was characterized by parameters  $A_{\max}$ ,  $t_{1/10}$ ,  $p$  and  $k_{\text{obs}}$ , as described by Bonfils *et al* [28].  $A_{\max}$  is the maximum absorbance plateau value measured in the assay, and reflects polymerized tubulin amount.  $t_{1/10}$  is the abscissa value of the  $A_{\max}/10$  absorbance.  $p$  is the slope of the plot  $\log(A(t)/A_{\max})$  versus  $\log(t)$  during the elongation process, *ie* from 1 min to the time of 80%  $A_{\max}$ . The value of  $p$  is indicative of the number of successive steps in the nucleation process. The pseudo-first order rate constant of elongation,  $k_{\text{obs}}$ , is determined by plotting  $\ln(1 - A(t)/A_{\max})$  as a function of time.

### Microtubule network observation by immunofluorescence

A375 cells plating and treatment were the same as described for proliferation kinetics. A375 cell line was treated for 24h with EAPB0203, EAPB0503 and imiquimod at various concentrations (2 and 5 times their respective  $IC_{50}$  as determined in A375 cells). Colchicine (1  $\mu\text{M}$ ) was used as positive control. Culture medium with a similar DMSO concentration was used as negative control. Interphase microtubule network was visualized by direct immunofluorescence. Culture medium was removed and cells fixed with methanol. Cells were then incubated with a mouse monoclonal anti- $\beta$ -tubuline antibody (Mouse clone TUB 2.1, T4026, Sigma-Aldrich) for 1.5h, followed by incubation with a secondary Rhodamine-labeled anti-mouse antibody for 1.5h. After washing, cells were colored with Hoechst (Life Technologies, Saint-Aubin, France). Microtubule network (green) and nuclear DNA (red) were visualized using a Leica DMRM fluorescence microscope with a 63x magnification. Images were obtained using a JAI CV-M1 camera and Isis software, and merged using Adobe photoshop software.

### Combination with colchicine and vinorelbine for cytotoxicity

A375 cells were seeded in 96 well-plates at 20,000 cells per well. Treatment was applied 24 hours later. Control cells received culture medium only. Higher concentrations for the test were chosen based on previously determined  $IC_{50}$  values, and were  $2.81 \times 10^{-5}\text{M}$  for EAPB0203,  $1.6 \times 10^{-6}\text{M}$  for EAPB0503,  $1.34 \times 10^{-7}\text{M}$  for colchicine,  $3.06 \times 10^{-4}\text{M}$  for vinorelbine, and  $1.17 \times 10^{-4}\text{M}$  for imiquimod (for  $IC_{50}$  evaluation method, see [16]). For each combination test, cells were treated with each compound alone and with the constant ratio combination, at the higher concentrations chosen and concentrations obtained by nine serial half dilutions. Cell viability was assessed 48h after treatment, using the 3-(4,5-Dimethyl-2-thiazolyl)-2,5-diphenyl-2H-tetrazolium bromide (MTT) test. Chou and Talalay method was used to calculate a combination index [29,30], using the CalcuSyn software (Biosoft, Cambridge, UK). Briefly, the median effect equation correlates the drug dose to cytotoxicity as follows:

$$fa/fu = (D/Dm)^m$$

where  $D$  is the dose,  $Dm$  is the dose necessary to obtain the median effect,  $fa$  is the fraction affected by the dose and  $fu$  is the fraction unaffected by the dose ( $fu = 1 - fa$ ), and  $m$  embodies the sigmoidicity of the dose-effect curve. This equation is used to calculate  $Dx$ , the dose that kills  $x\%$  of cells. The Combination Index (CI) is then calculated as follows:

$$CI = (D)_1/(Dx)_1 + (D)_2/(Dx)_2$$

$CI < 1$ ,  $CI = 1$  and  $CI > 1$  respectively mean a synergy, an additive effect or an antagonism.

## Molecular modeling of interaction with tubulin

Molecular docking *in silico* was used to investigate the possible binding modes of EAPB0203, EAPB0503 and imiquimod on the colchicine binding site of tubulin. The AutoDock Vina program was used [31]. AutoDock Tools [32] was used for tubulin (PDB1SA0, *Bos taurus*) and ligands preparation to generate pdbqt files. Water molecules and colchicine were removed from PDB1SA0, polar hydrogens and Gasteiger partial charges were added. Ligands were obtained on the data base ZINC [33] in.mol2 files, and prepared the same way, with assignment of all flexible covalent bonds. A grid of 40x40x40 points in x,y,z axes and a space of 0.375 Å was centered on colchicine binding site (center: 116, 556x89, 199x6,541). For each run, the first ten more stable conformations were considered. Docking results were handled using the opensource PyMOL Molecular Graphics System, Version 1.7.4 Schrödinger, LLC. Predicted binding affinity is calculated based on the score function used by Autodock Vina ( $\Delta G = \Delta G_{H\text{-bond}} + \Delta G_{vdw} + \Delta G_{\text{hydrophobic}} + \Delta G_{\text{conformation}}$ ), which is composed of a conformation-dependent component (including intra- and intermolecular steric, hydrophobic and hydrogen interactions) and a conformation-independent component (taking into account the number of rotative bonds between ligands atoms). Each contribution is given a different weight to score function [34].

## Competition with colchicine for tubulin binding: Fluorescence of the colchicine-tubulin complex

We used an intrinsic property of colchicine, which makes a fluorescent complex when bound to tubulin ( $\lambda_{\text{exc}} = 365\text{nm}$ ,  $\lambda_{\text{em}} = 435\text{nm}$ ) but is not fluorescent in solution [35]. Tubulin (3  $\mu\text{M}$ ) was incubated with colchicine (3  $\mu\text{M}$ ) for 30 minutes at 37°C to form complexes. EAPB0203, EAPB0503, imiquimod, nocodazole (positive control) and vinorelbine (negative control) were then added at different concentrations (5, 15, 20 and 30  $\mu\text{M}$ ), then incubated for 60 minutes at 37°C. Fluorescence spectra were recorded after excitation at 365 nm. Fluorescence was corrected for blank and imiquimod slight fluorescence when necessary with equimolar solutions.

## Data analysis

Linear regressions and statistical tests were performed using GraphPad Prism software (GraphPad Software, Inc., La Jolla, USA).

## Results

### EAPB0203 and EAPB0503 inhibit cell proliferation and display cytotoxicity

EAPB0203 and EAPB0503 at the highest concentration tested (5 and 0.5  $\mu\text{M}$  respectively) totally inhibited A375 cell growth until 72h (Fig 2), the number of cells decreasing slightly with time. When used at the lowest concentration (0.5 and 0.05  $\mu\text{M}$  respectively), EAPB0203 and EAPB0503 had no effect on cell proliferation kinetics. Interestingly, EAPB0503 at 0.5  $\mu\text{M}$  concentration had a similar effect as EAPB0203 at 5  $\mu\text{M}$ , confirming its roughly ten times higher cytotoxic activity.

### EAPB0203 and EAPB0503 block cell cycle in G2 and M phases and induce apoptosis

Nocodazole 50 ng/mL used as positive control led to 37.8% (Standard Deviation (SD) 9.87) cells blocked in M phase after 16h treatment. EAPB0203 and EAPB0503, respectively at 5 and

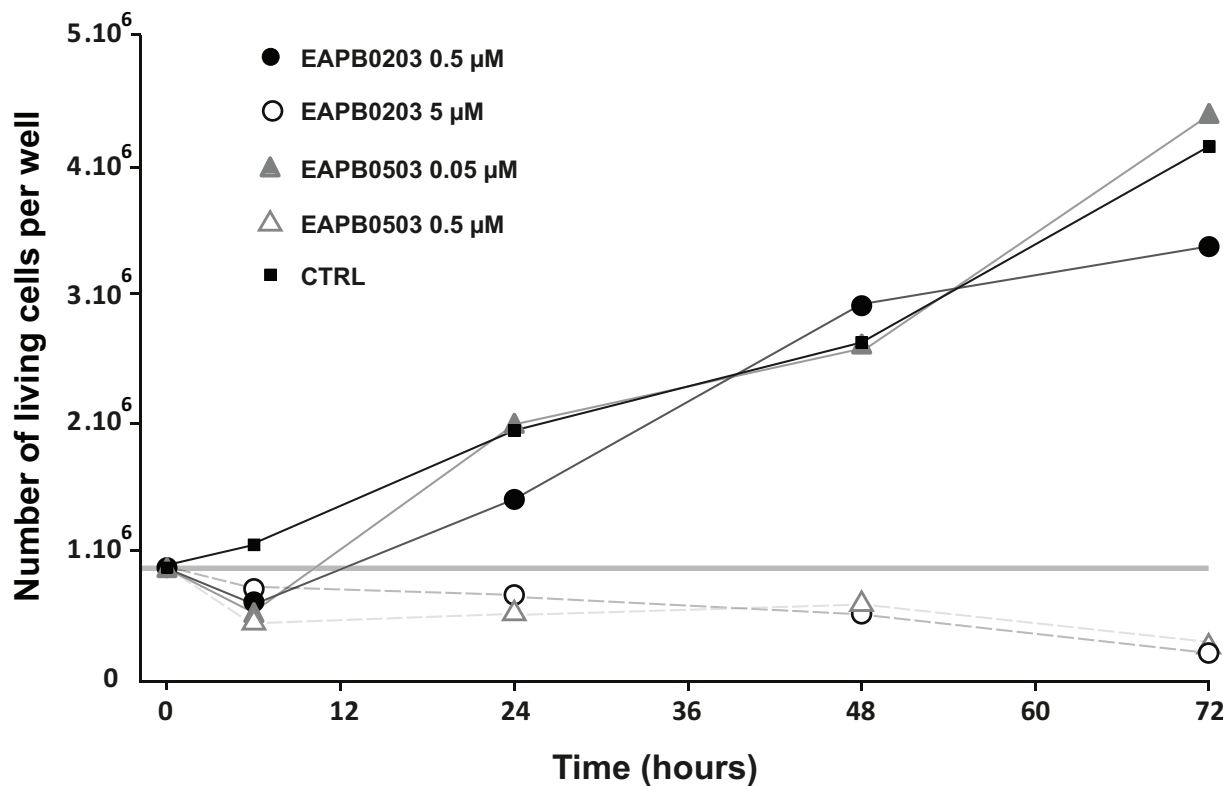


**Fig 2. EAPB0203 and EAPB0503 inhibit cell proliferation and display cytotoxicity.** A375 cells were treated with EAPB0203 or EAPB0503 at the indicated concentrations, harvested at various times post-treatment, and counted using Casy cell counter. Percentage of dead cells was determined on Malassez hemocytometer after trypan blue staining, and dead cells removed from the total cell count. The thick grey line corresponds to the number of living cells as counted at time zero.

<https://doi.org/10.1371/journal.pone.0182022.g002>

0.5  $\mu$ M, induced accumulation of treated A375 cells in G2/M and M phase after 24h (Fig 3). Proportion of cells in G2/M grew from 23.0% (negative control) to 56.9% (EAPB0203 5  $\mu$ M) and 54.9% (EAPB0503 0.5  $\mu$ M). Consistently, proportion of cells in M grew from 2.35% to 22.7% and 23.4% respectively. Accumulation in M was not sufficient to account for G2/M accumulation, suggesting also G2 accumulation. Increase in mitotic index was associated with a decrease in cells in G0/G1 (first Peak), as illustrated in S2 Fig. Accumulation of treated cells in G2/M and M phases was negligible at 48h, and totally disappeared at 72h. EAPB0203 5  $\mu$ M induced apoptosis in more than 20% of the cells after 48 and 72h, while percent of apoptotic cells remained below 5% for untreated cells (Fig 3). Percent of necrotic cells strikingly increased from 13.8% after 48h to 25% after 72h, while the maximum percent of dead cells for untreated cells was 11.2% after 72h. A similar trend was observed for EAPB0503 0.5  $\mu$ M, but the percent of apoptotic cells reached 41.6% after 72h. Representative cytometry results are displayed in S3 Fig.

### EAPB0203, EAPB0503 and imiquimod bind tubulin

A SPR approach was used to evaluate the direct binding of EAPB0203, EAPB0503 and imiquimod to tubulin immobilized on a CM5 sensor chip. The experiment was validated by a dose effect experiment performed on colchicine (S4 Fig). The resulting  $K_D$  of 21  $\mu$ M was in accordance with the literature [36]. As expected, warfarin showed no binding to tubulin with no detectable signal. A specific dose-dependent binding to tubulin was observed for EAPB0203,

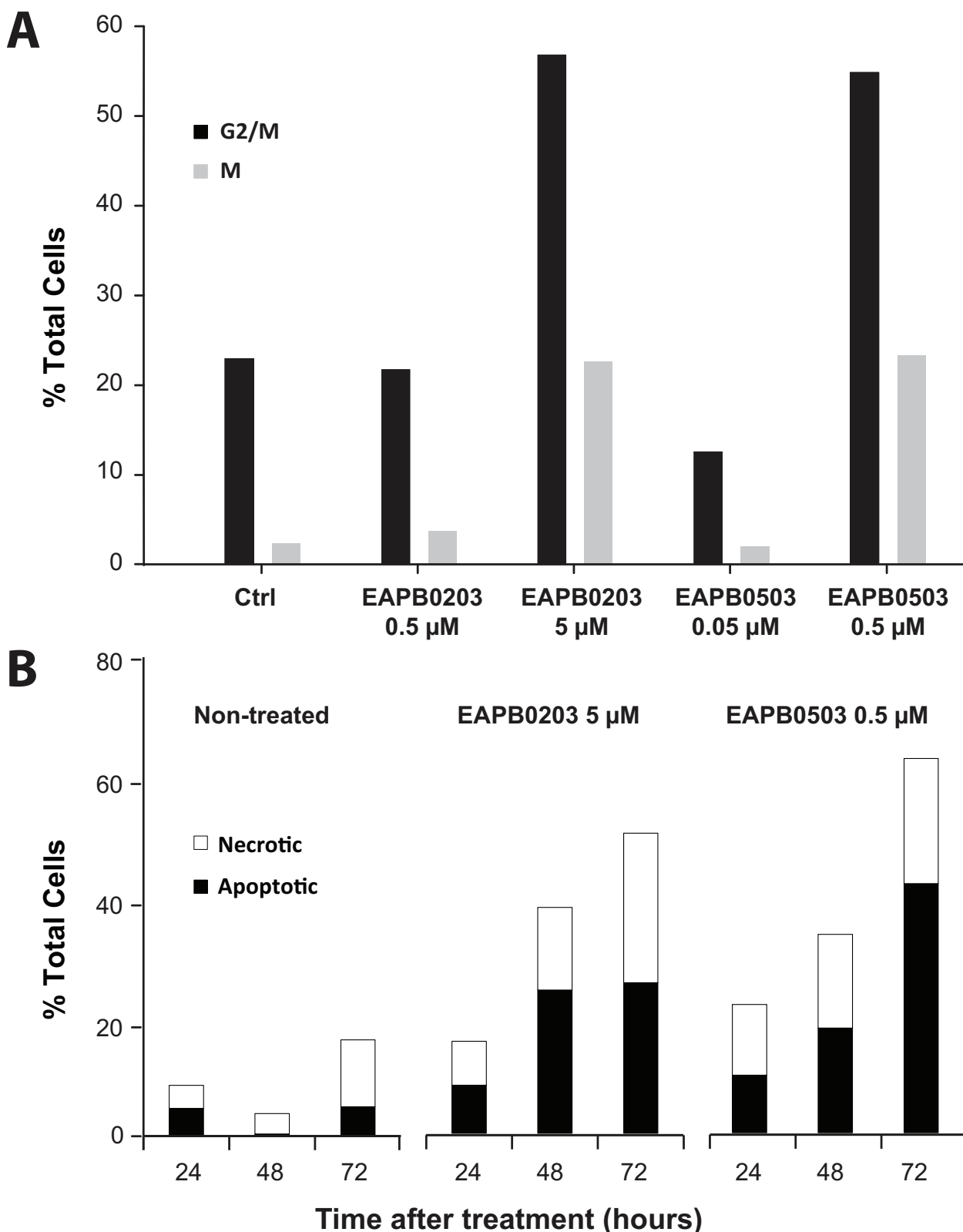


**Fig 3. EAPB0203 and EAPB0503 block cell cycle in G2 and M phases and induce apoptosis.** A375 cells were treated with EAPB0203 or EAPB0503 at the indicated concentrations. (A) After 24 hours, cells were stained with propidium iodide alone (G2/M) or

with propidium iodide and anti-phospho histone H3 antibody (M). Flow cytometry was used to determine the percentage of cells in G2/M and M phases of the cell cycle. (B) After the indicated time, cells were stained with 7-AAD and Annexin V. We used flow cytometry to determine the percentage of necrotic and secondary necrotic cells (Annexin V and 7-AAD positive) and early stage apoptotic cells (Annexin V positive and 7-AAD negative).

<https://doi.org/10.1371/journal.pone.0182022.g003>

EAPB0503 and imiquimod (Fig 4). A linear regression was performed between test compound concentrations and binding response. Slope was significantly different from zero for imiquimod, and EAPB0503, but not EAPB0203. The binding responses of test compounds were higher than colchicine responses (Fig 4), but under or equal to the calculated stoichiometric binding level (20–25 RU).  $K_D$  could not be determined due to higher concentration limit associated to aggregation.

### EAPB0203, EAPB0503 and imiquimod inhibit purified tubulin polymerization

As shown in Fig 5, at concentrations lower than or equal to 10  $\mu$ M, EAPB0203 and EAPB0503, as well as colchicine, dose-dependently inhibited polymerization of tubulin, while imiquimod had no effect. Indeed, the parameter  $A_{max}$ , considered as proportionally related to the mass concentration of tubulin polymer [28], was decreased by EAPB0203, EAPB0503 and colchicine. Strength of the effect was differential, with EAPB0503 > colchicine > EAPB0203. Polymerization was totally prevented by colchicine at 10  $\mu$ M, and EAPB0503 at 5 and 10  $\mu$ M.

Nucleation process seemed to be delayed by EAPB0203 and EAPB0503, but not colchicine, as reflected by the increase in  $t_{1/10}$ , while no effect was observed on  $p$  parameter. The pseudo-first order elongation rate  $k_{obs}$  was decreased by EAPB0203 and EAPB0503, but not colchicine, suggesting a slowdown and impairment of elongation process. Since imiquimod IC<sub>50</sub> in A375 cells (70.3  $\mu$ M) was much higher than IC<sub>50</sub> of EAPB0203 or EAPB0503 (1.57 and 0.2  $\mu$ M respectively) [11], we assessed the effect of imiquimod on tubulin polymerization at higher imiquimod concentrations. From 320  $\mu$ M, imiquimod decreased  $A_{max}$  and  $k_{obs}$ , and increased

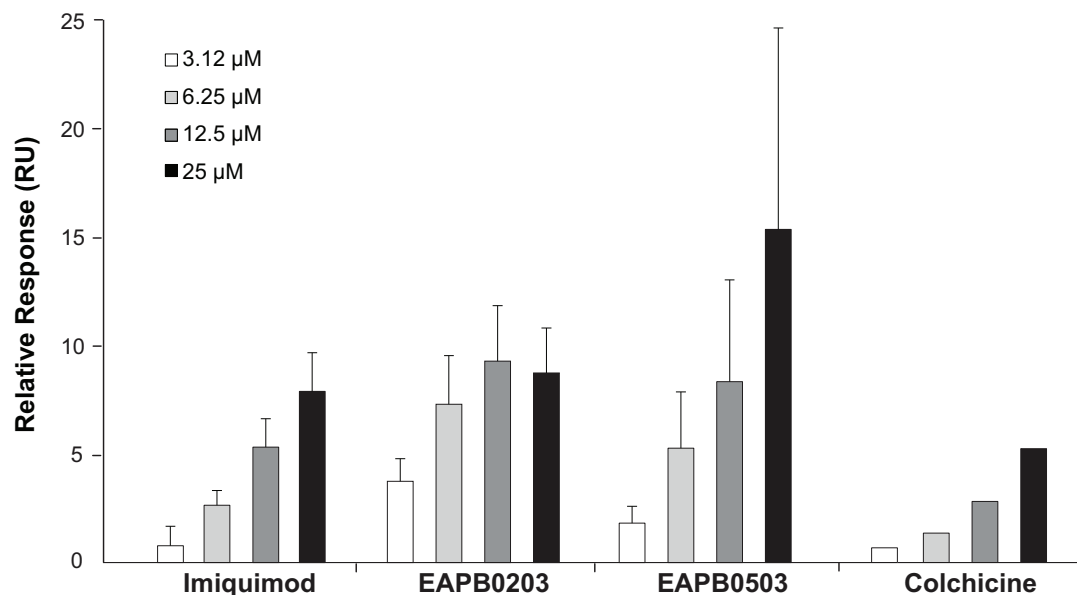


**Fig 4. EAPB0203, EAPB0503 and imiquimod bind tubulin.** Binding levels of EAPB0203, EAPB0503 and imiquimod were determined by surface plasmon resonance on immobilized tubulin at different concentrations (n = 4, except for colchicine n = 1).

<https://doi.org/10.1371/journal.pone.0182022.g004>

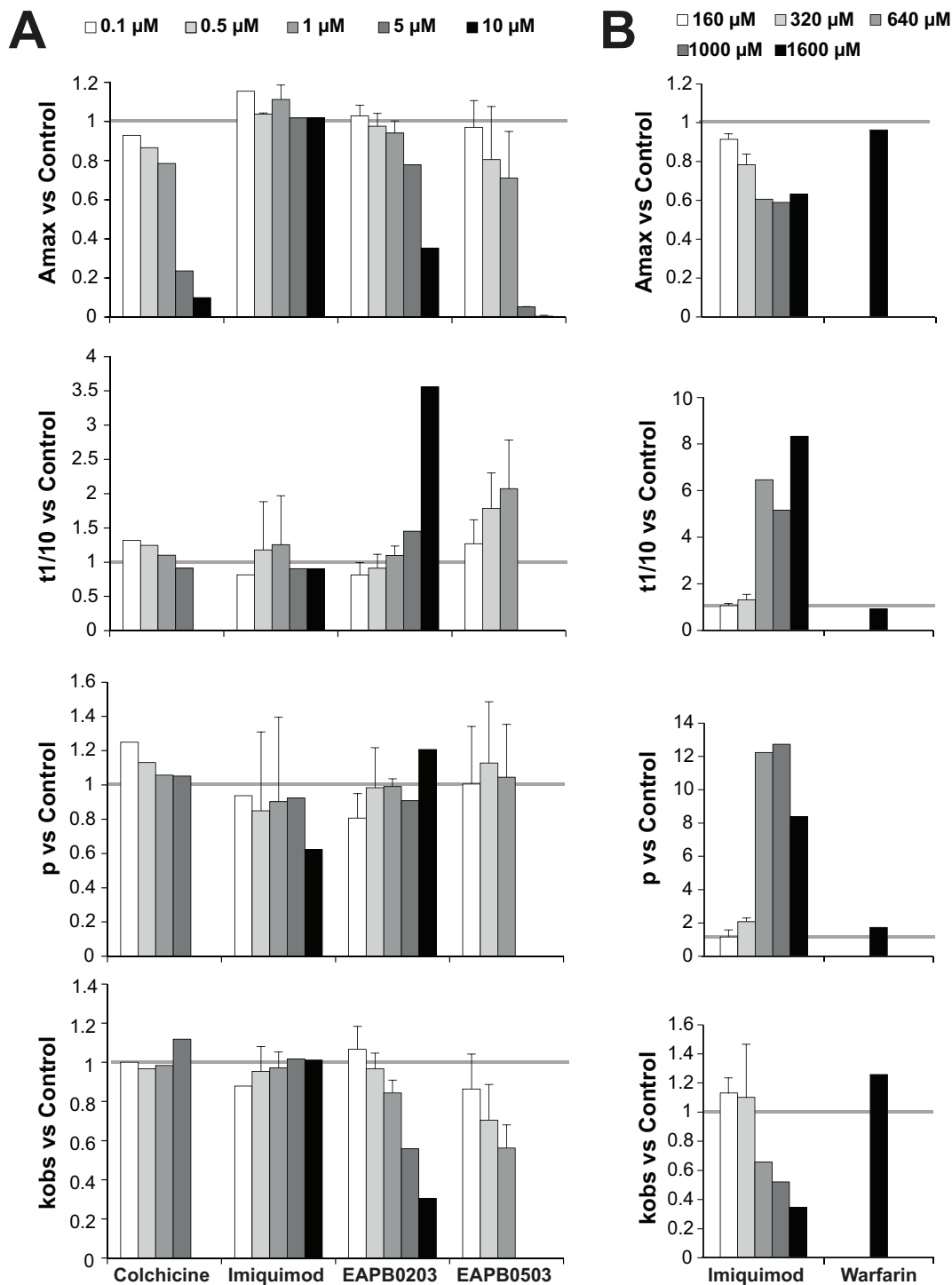


**Fig 5. EAPB0203 and EAPB0503, and imiquimod at high concentrations, inhibit polymerization of tubulin *in vitro*.** Purified tubulin polymerization was quantitated by turbidimetry measurement at 350 nm with or without (blank) various concentrations of EAPB0203, EAPB0503, imiquimod, and colchicine as positive control, or warfarin (1,600 μM) as negative control. Various parameters representative of the polymerization process were calculated:  $A_{max}$  (maximum absorbance plateau value),  $t_{1/10}$  (abscissa value of the  $A_{max}/10$  absorbance),  $p$  (slope of the plot  $\log(A(t)/A_{max})$  versus  $\log(t)$  during the elongation process, i.e. from 1 min to the time of 80%  $A_{max}$ ), and  $k_{obs}$  (pseudo-first order rate constant of elongation, determined by plotting  $\ln(1 - A(t)/A_{max})$  as a function of time). The ratio to blank values are reported here. The red line embodies the ratio of 1, meaning identity to blank. Mean  $\pm$  SD,  $n = 1$  to 6. (A) EAPB0203, EAPB0503, imiquimod and colchicine at 0.1 to 10 μM concentrations. (B) Imiquimod at 160 to 1,600 μM concentrations. Mean  $\pm$  SD,  $n = 1$  or 2.

<https://doi.org/10.1371/journal.pone.0182022.g005>

$t_{1/10}$  and  $p$  (Fig 5). Hence, imiquimod's effect on tubulin polymerization displayed the same profile as EAPB0203 and EAPB0503, except for the increase in  $p$ , suggestive of an increase of nucleus size. A linear regression was performed between test compound concentrations and each polymerization parameter, which confirmed our observations. Indeed, for  $A_{max}$ ,  $t_{1/10}$  and  $k_{obs}$ , slope was significantly different from zero for imiquimod, EAPB0203 and EAPB0503. For the parameter “ $p$ ”, slope was significantly different from zero for imiquimod only.

### EAPB0203, EAPB0503 and imiquimod disturb microtubule network in A375 cells

A homogeneous well-defined microtubule network was observed for control cells, with microtubules orientated from the center to the periphery of the cell. Many mitotic cells with a mitotic spindle were visualized. EAPB0203, EAPB0503 and imiquimod markedly disorganized the microtubule network at a concentration of 5 times their respective  $IC_{50}$  (Fig 6), in a manner that differed from colchicine, which totally prevented microtubule polymerization (S5 Fig). The cytoskeleton was inhomogeneously distributed, morphology was rounder, and adhesion to coverslips was reduced, which might be associated to destabilization of tubulin cytoskeleton. Later than 24h, very few mitotic cells could be observed, consistently with apoptotic death of cells blocked in M as evaluated by flow cytometry. These qualitative observations illustrate that, in addition to interacting with purified tubulin *in vitro*, the test compounds also modify microtubule structure in cells.

### EAPB0203, EAPB0503 and imiquimod display an antagonist cytotoxic effect with colchicine

Most compounds that inhibit tubulin polymerization bind two major domains of tubulin: vinca and colchicine domains [37,38]. In order to identify whether EAPB0203 and EAPB0503 would bind one of those well-identified sites, we combined them with colchicine and vinorelbine and measured the effect of the combination on cytotoxicity in A375 cells. Chou-Talalay method was used to calculate a combination index (CI) with Calcsyn software [29,30]. After calculation of CI at various concentrations (Fig 7), we found that EAPB0203, EAPB0503 and imiquimod were acting antagonistically to colchicine on cytotoxicity ( $CI > 1$ ). A synergistic effect was oppositely obtained with vinorelbine ( $CI < 1$ ), which was less clear for imiquimod. Consistently, a synergistic effect has been described for vinorelbine and colchicine combination [39]. These results strongly suggest that EAPB0203, EAPB0503 and imiquimod might bind tubulin on the colchicine binding site, and not on the vinca-alcaloids binding site.

### EAPB0203, EAPB0503 and imiquimod can bind tubulin on the colchicine-binding site

To confirm the hypothesis raised by SPR and combination studies, we first investigated the possible binding modes of EAPB0203, EAPB0503 and imiquimod on the colchicine binding site of beta-tubulin, using molecular docking *in silico*. The docking method was validated by redocking colchicine on the colchicine binding site: the experimental crystallography conformation and the lowest energy conformation predicted by Autodock Vina were similar (RMSD of 0,568 Å between the two structures) (S6 Fig). Among the binding modes generated for EAPB0203, EAPB0503 and imiquimod, the lowest energy modes corresponded to a superposition with colchicine (Fig 8).

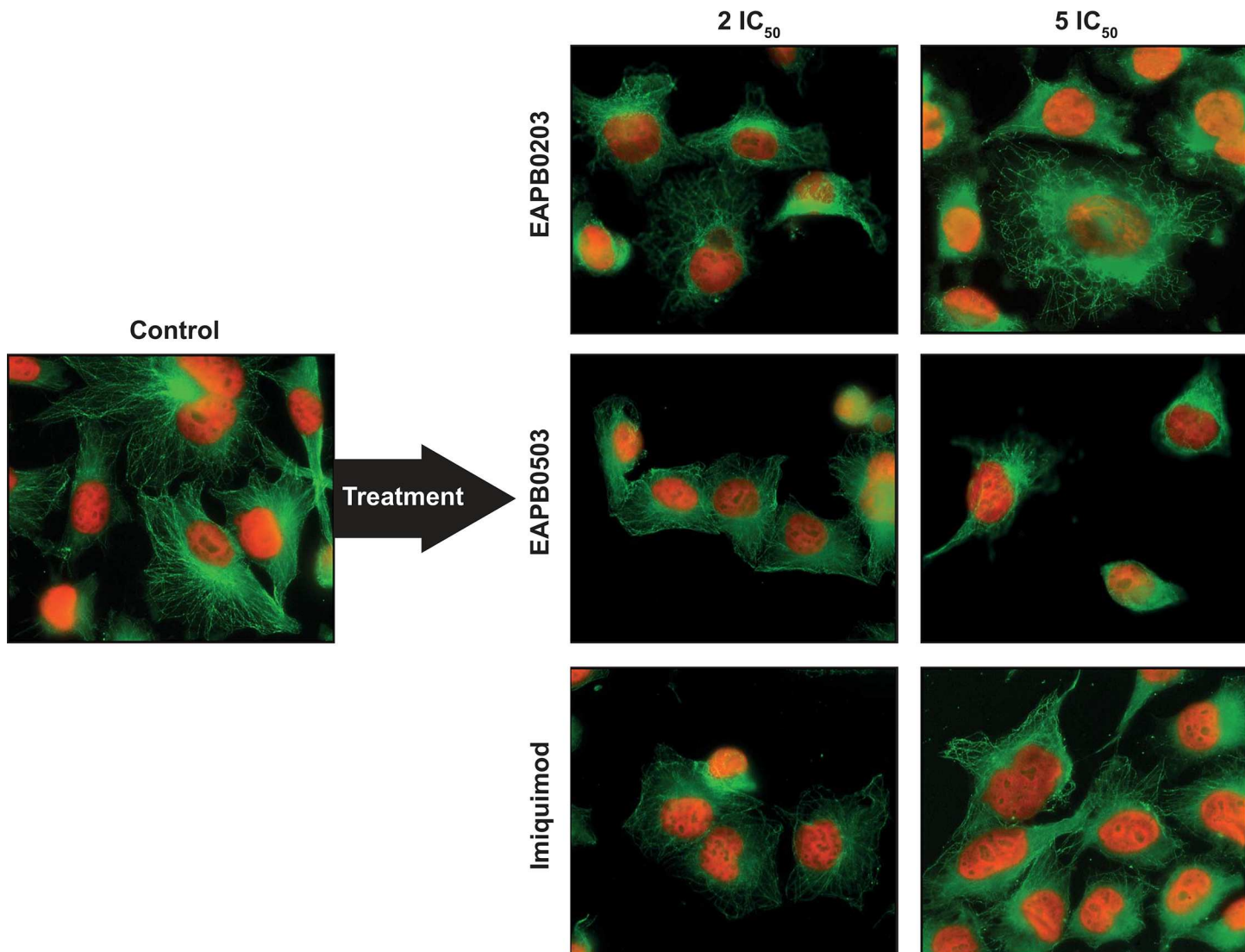


**Fig 6. EAPB0203, EAPB0503 and imiquimod disturb microtubule network in A375 cancer cell line.** A375 cells were treated by EAPB0203, EAPB0503 and imiquimod at the indicated concentrations for 24h. Beta-tubulin was stained using a mouse monoclonal anti- $\beta$ -tubulin antibody and a secondary Rhodamine-labeled anti-mouse antibody. Nuclei were stained with Hoechst. Microtubule network (green) and nuclear DNA (red) were visualized using a Leica DMRM fluorescence microscope with a 63x magnification. Representative images are displayed here.

<https://doi.org/10.1371/journal.pone.0182022.g006>

Twenty-nine residuals were identified as being involved in colchicine binding to beta-tubulin [40]. The C ring of colchicine interacts with a specific zone (labeled in orange in Fig 8) through Van Der Waals contacts with Val $\alpha$ 181, Ser $\alpha$ 178, and Val $\beta$ 315. Interestingly, the same hydrophobic interactions were involved for EAPB0503 and EAPB0203, and to a lower extent for imiquimod, which does not contain a phenyl ring. Colchicine ring A is buried in a second hydrophobic pocket (labeled in blue in Fig 8). The methoxy group in 3 position is involved in a hydrogen bond with the thiol group of Cys $\beta$ 241. This conformation was also found for EAPB0203, EAPB0503 and imiquimod, whose quinoxaline and quinoline aromatic rings are in close contact with Cys $\beta$ 241. A similar conformation is frequently found among colchicine site pharmacophores, and is considered essential to activity [41]. Moreover, the conformation obtained is compatible with hydrophobic contacts between methylamine group and Ala $\beta$ 250

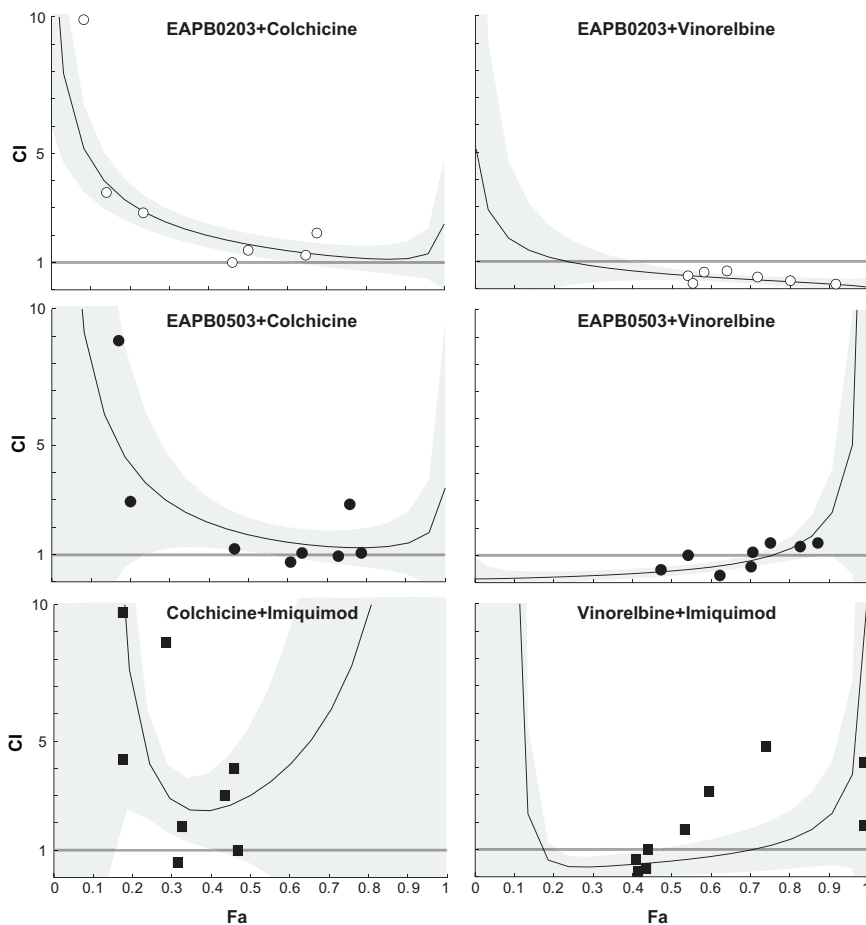


**Fig 7. EAPB0203, EAPB0503 and imiquimod display an antagonistic effect with colchicine, but synergistic with vinorelbine.** A375 cells were treated with EAPB0203, EAPB0503, colchicine and vinorelbine—alone and with constant ratio combination—at concentrations surrounding their previously determined  $IC_{50}$ . Cell viability was assessed 48h after treatment, using the MTT test. Chou and Talalay method was used to calculate a combination index:  $CI < 1$ ,  $CI = 1$  and  $CI > 1$  respectively mean a synergy, an additive effect or an antagonism. The grey frame embodies the 90% confidence interval as determined by CalcuSyn software.  $Fa$  = fraction affected by the dose.

<https://doi.org/10.1371/journal.pone.0182022.g007>

and  $Leu\beta 242$ , and with an hydrogen bond to  $Cys\beta 241$  (3.4 Å), which could explain the higher biological activity of EAPB0203 and EAPB0503 when compared to other compounds of the imidazo[1,2-*a*]quinoxalines family with a different substitution [9]. In the case of colchicine, in addition to the hydrogen bond to  $Cys\beta 241$ , a carbonyl group on the C ring is involved in a hydrogen bond to  $Val\alpha 181$ . This highly energetic bond to  $Val\alpha 181$  is also found for EAPB0503, whose lowest energy conformation shows a favorable position of methoxyphenyl (3.1 Å). Autodock Vina algorithm predicts similar affinity for colchicine (score of -9.1 kcal/mol), EAPB0203 and EAPB0503 (both -8.9 kcal/mol), while imiquimod displays less affinity (-7.3 kcal/mol).

To confirm the involvement of the colchicine binding site of beta-tubulin in the interaction of EAPB0203, EAPB0503 and imiquimod with tubulin, we studied the competition of EAPB0203, EAPB0503 and imiquimod with colchicine for tubulin binding. When nocodazole (used as positive control of colchicine site binding) but also EAPB0203, EAPB0503 and imiquimod were added to colchicine and tubulin, fluorescence decreased dose-dependently (Fig 8),

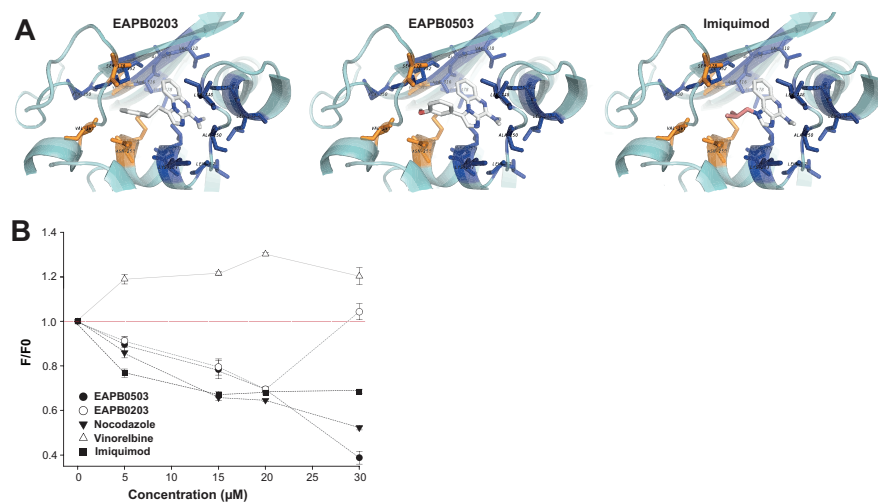


**Fig 8. EAPB0203, EAPB0503 and imiquimod bind tubulin on the colchicine binding site.** (A) Interaction modes of EAPB0203, EAPB0503 and imiquimod on the colchicine site as predicted by AutoDock Vina. Molecules interact with two hydrophobic pockets (blue and orange). (B) Competition of EAPB0203, EAPB0503, imiquimod, nocodazole (positive control) and vinorelbine (negative control) with colchicine for tubulin binding. Fluorescence of the colchicine-tubulin complex was measured after excitation at 365 nm. F/F0: relative fluorescence intensity, F0: fluorescence intensity of the colchicine-tubulin complex alone.

<https://doi.org/10.1371/journal.pone.0182022.g008>

suggesting that these molecules were competing with colchicine for binding to tubulin. Contrarily, vinorelbine, which binds to another site, did not decrease fluorescence, and actually increased fluorescence, suggesting a potential synergistic action. Addition of 30  $\mu$ M EAPB0203 induced no reduction of fluorescence, which might be related to aggregation phenomena disturbing the fluorescent signal (S1 Fig). These results strongly suggest that EAPB0203, EAPB0503 and imiquimod bind tubulin on the colchicine site.

## Discussion

Anti-microtubule agents are known to target the tubulin cytoskeleton and suppress microtubule dynamics, which leads to aberrant mitotic spindle, cell cycle blockade in G2/M phases, and finally induces apoptotic cell death [38]. Consistently, through a cluster of complementary results, we demonstrated in the present paper that EAPB0203 and EAPB0503, strong antiproliferative agents from the imidazo[1,2-*a*]quinoxalines series, display an anti-microtubule activity. First, we observed that EAPB0203 and EAPB0503 impaired A375 cell proliferation, blocked cell cycle in G2 and M phases, and induced apoptotic cell death. Second, we showed that EAPB0203 and EAPB0503 dose-dependently inhibited purified tubulin polymerization in a cell-free system, with a strength similar to colchicine, and at cellular level demolished microtubule network organization in A375 cell line. Finally, we demonstrated that EAPB0203 and EAPB0503 bound tubulin and interacted with the colchicine binding site. SPR analysis showed a direct dose-dependent specific binding to tubulin. Our molecular docking data suggested an interaction with the colchicine-site of  $\beta$ -tubulin, which was confirmed by colchicine-site binding competition studies. The latter finding was in line with combination studies, which showed an antagonistic cytotoxic effect of EAPB0203 and EAPB0503 with colchicine, but a synergistic cytotoxic effect with vinorelbine.

The present findings are consistent with previously published results regarding the mode of action of EAPB0203 and EAPB0503. EAPB0503 has recently been shown to inhibit tubulin polymerization [25]. EAPB0203 and EAPB0503 have been shown to impair cell growth, block

cell cycle in G2/M phase, and induce apoptosis in ATLL cells (EAPB0203) and CML cells (EAPB0503). Furthermore, as shown in malignant T cells, EAPB0203 negatively regulated c-IAP-1 and Bcl-XL anti-apoptotic proteins, stabilized p53 and p21 pro-apoptotic proteins, and activated p38MAPK pathway [12]. Similar downstream regulation of p53, p21, c-IAP, Bcl-XL and MAPK has been described for anti-microtubule agents [42,43]. These findings are in favor of a close cause consequence relationship between antimicrotubule activity and the cytotoxicity mechanisms observed with these compounds. We envision that our next studies could benefit from further identification of the effects that contribute the most to cytotoxicity through a concentration dependent comparative analysis of cellular effects, which could in turn guide pharmacomodulation and inform on the pharmacological potential of these compounds. Due to their role in mitosis and cell division, microtubules and their dynamics are a major target for anticancer drugs, cancer cells being more vulnerable due to a higher rate of division [44]. Based on the success of the chemically diverse class of anti-microtubule drugs (with various tubulin-binding sites), it has been argued that microtubules represent the best cancer target identified so far. It seems likely that drugs of this class will continue to be major chemotherapeutic agents, despite the development of more selective approaches [44,45]. More specifically, the colchicine-site has been described as one of the most important target for tubulin polymerization inhibitors. In the hope of developing novel useful drugs with favorable pharmacological profiles, a large number of molecules with structural diversity has been identified as interacting with the colchicine site of tubulin and some have been shown to exert an anticancer activity by leading to G2 arrest and apoptosis [46,47]. For example, the molecule BAL27862 is currently in phase I clinical trial [48]. To our knowledge, among described pharmacophores of tubulin colchicine domain [48,49], no structure is related to imidazoquinoxaline structure. EAPB0203 and EAPB0503 hence represent unique colchicine domain binding compounds. In spite of the recent discovery of many novel pharmacophores, increasing the library of available compounds could facilitate the identification of appropriate pharmacokinetic properties in order to obtain a highly potent, low toxicity anti-microtubule agent for the treatment of cancers.

A totally unexpected and nevertheless major result was also obtained in the present study: we happened to observe for the first time that the marketed drug imiquimod might bind to the colchicine-binding site of tubulin, and could accordingly inhibit tubulin polymerization, although at higher concentrations than EAPB0203 and EAPB0503. Imiquimod was not included in proliferation, cell cycle or apoptosis tests because it displays a very low cytotoxicity in A375 cells ( $IC_{50}$  70.3  $\mu$ M), which is consistent with the insubstantial induction of cell death by imiquimod alone reported by Weber *et al.* [50]. Imiquimod was initially included in tubulin binding SPR assays as a negative control, which led to the unexpected discovery that imiquimod actually also bound tubulin. Imiquimod is a marketed and well-known drug. The main mechanism of action of imiquimod is associated to immune stimulation involving alpha-interferon induction [51] through modulation of Toll-like receptor 7 (TLR7) [52]. A direct pro-apoptotic effect of imiquimod has also been described in various skin cancer cell types, including melanoma, and involved the mitochondrial pathway of apoptosis, as suggested by Bcl-2-dependent cytosolic translocation of cytochrome c [53,54]. Treatment with imiquimod was also reported to induce cell cycle arrest at the G2/M phase in TRAMP-C2 mouse prostate cancer cells, and apoptosis via the mitochondrial-dependent pathway [55]. Consistently with our results, the above studies were conducted at high concentrations of imiquimod, at least 5  $\mu$ g/mL (i.e. 20.8  $\mu$ M, imiquimod weighing 240.3 g/mol). Although not formally demonstrating a causative link between interaction with tubulin and cytotoxic activity, we observed that the concentrations needed to inhibit tubulin polymerization (0.5, 5 and 320  $\mu$ M for EAPB0503, EAPB0203 and imiquimod respectively) were in the same range as the cytotoxic concentrations (0.2, 1.57 and 70.3  $\mu$ M for EAPB0503, EAPB0203

and imiquimod respectively) for the three molecules evaluated. In contrast, and as could be expected, effect on tubulin polymerization was not correlated to TLR7 agonist activity, which was observed at a much lower concentration for imiquimod (from 1  $\mu$ g/mL or 4.16  $\mu$ M) while no TLR7 agonist activity was observed for EAPB0203 and EAPB0503 even at 100  $\mu$ g/mL (above 300  $\mu$ M) (S7 Fig). However, as stated by Narayan *et al.* [22], the exact mechanism of action of imiquimod is still largely undefined. We discovered that imiquimod bound to tubulin and was able to inhibit purified tubulin polymerization. Furthermore, our results are consistent with the binding of imiquimod to the colchicine site of tubulin. To our knowledge, no interaction between imiquimod and tubulin had been reported before. Even though further studies are needed to confirm this interaction, our results bring a new stone to the understanding of the mechanism of action of imiquimod.

## Supporting information

**S1 Fig. Aggregation of EAPB0203, EAPB0503, colchicine and imiquimod as evaluated using dynamic light scattering.** We measured the mean particle size of EAPB0203, EAPB0503 and imiquimod at different concentrations in HBS-EP+ buffer which was used in the SPR experiments presented in Fig 4. After dissolving the compounds with sonication, the solutions were allowed to equilibrate for 2 hours. Experiments were limited by aggregation phenomenon, which occurred for EAPB0203 above 25  $\mu$ M with an increased particle size and a polydispersity index superior to 0.7.

(EPS)

**S2 Fig. Representative dot plot of cells in G2/M and M phases measured by flow cytometry, used to elaborate Fig 3A.** A375 cells were treated with using Phospho-Histone H3 (phycoerythrin conjugate, PE) and propidium iodide (PI) as described in Materials and methods. Flow cytometry analysis was performed with FACS Calibur 2, using two fluorescence channels. Cells in G2/M (stained with PI) and in M (stained with PI and anti-PH3) phases were then analyzed using FlowJo software.

(EPS)

**S3 Fig. Representative dot plot of dead and apoptotic cells measured by flow cytometry, used to elaborate Fig 3B.** A375 cells were harvested 24, 48 and 72 hours after treatment and double-stained using Annexin V-FITC /7-AAD kit as described in Materials and methods. Flow cytometry analysis and quantitation of dead cells (Annexin V and 7-AAD positive) and apoptotic cells (Annexin V positive and 7-AAD negative) were performed using the FlowJo software.

(EPS)

**S4 Fig. Evaluation of the affinity of colchicine to tubulin as measured by surface plasmon resonance.** Kinetic response profile (A), and maximum response plotted against concentration of Colchicine (B). This dose effect experiment performed on colchicine enabled us to calculate a resulting  $K_D$  of 21  $\mu$ M, in accordance with the literature, which permitted to validate our experimental set up to measure the affinity of EAPB0203, EAPB0503 and imiquimod to tubulin.

(EPS)

**S5 Fig. Colchicine (1  $\mu$ M) prevents microtubule polymerization in A375 cancer cell line after 24h.** Beta-tubulin was stained using a mouse monoclonal anti- $\beta$ -tubulin antibody and a secondary Rhodamine-labeled anti-mouse antibody. Nuclei were stained with Hoechst. Microtubule network (green) and nuclear DNA (red) were visualized using a Leica DMRM

fluorescence microscope with a 63x magnification. Two representative images are displayed here.

(EPS)

**S6 Fig. Comparison of natural crystallographic conformation (A) and conformation predicted by molecular docking (B) of colchicine on the colchicine site of beta-tubulin (PDB: 1SA0) using Autodock Vina. (C) Chemical structure of Colchicine.**

(EPS)

**S7 Fig. Evaluation of TLR7 agonist activity of EAPB0503, EPAB0203 and imiquimod, in comparison with the control TLR7/8 agonist R848 (resiquimod).** We observed activation of human and murine TLR7 reporters in HEK293 cells for imiquimod from 1  $\mu$ g/mL or 4.16  $\mu$ M, while no TLR7 agonist activity was observed for EAPB0203 and EAPB0503 even at 100  $\mu$ g/mL (above 300  $\mu$ M). (A) Dose response to human TLR7 on NF- $\kappa$ B reporter HEK293 (HEK-Blue™-hTLR7, Invivogen) (B) Dose response to murine TLR7 on NF- $\kappa$ B reporter HEK293 (HEK-Blue™-mTLR7, Invivogen).

(EPS)

**S1 File. Experimental raw data and images used to generate all figures.**

(ZIP)

## Acknowledgments

We are grateful to Dr Bernard Bourrié for his determining intellectual contribution to the project and his everyday support. We thank the Laboratory of Toxicology (P. Cuq, IBMM, CNRS UMR 5247, Montpellier, France) and BC2M (A-D Lajoix, EA7288, Montpellier, France) for allowing us to use their cell culture facilities. We thank J. Chopineau and J.-P. Moles for introducing us to new technics, and the staff of MRI platform (N. Vié, M. Boyer and C. Mon-gellaz) and PP2I platform (C. Henriet) for their availability. We also thank NCI/DTP Anti-Cancer Screening Program (<http://dtp.cancer.gov/>). Last we would like to thank Fabienne Vernejoul and Eric Perouzel (Cayla-Invivogen) for performing NF-KB reporter assays. The funders had no role in study design, data collection and analysis, decision to publish, or preparation of the manuscript.

## Author Contributions

**Conceptualization:** Alexis Courbet, Christian Larroque, Sonia Khier, Carine Deleuze-Masquefa, Florence Gattacceca.

**Data curation:** Alexis Courbet, Martine Pugniere, Safia El Messaoudi, Zahraa Zghaib, Florence Gattacceca.

**Formal analysis:** Alexis Courbet, Martine Pugniere, Safia El Messaoudi, Zahraa Zghaib, Florence Gattacceca.

**Funding acquisition:** Sonia Khier, Carine Deleuze-Masquefa, Florence Gattacceca.

**Investigation:** Nicole Bec, Christian Larroque, Sonia Khier, Carine Deleuze-Masquefa, Florence Gattacceca.

**Methodology:** Alexis Courbet, Nicole Bec, Caroline Constant, Christian Larroque, Martine Pugniere, Carine Deleuze-Masquefa, Florence Gattacceca.

**Project administration:** Carine Deleuze-Masquefa, Florence Gattacceca.

**Resources:** Christian Larroque, Martine Pugniere, Carine Deleuze-Masquefa, Florence Gattacceca.

**Software:** Alexis Courbet, Florence Gattacceca.

**Supervision:** Christian Larroque, Carine Deleuze-Masquefa, Florence Gattacceca.

**Validation:** Alexis Courbet, Caroline Constant, Christian Larroque, Martine Pugniere, Sonia Khier, Carine Deleuze-Masquefa, Florence Gattacceca.

**Visualization:** Alexis Courbet, Caroline Constant, Florence Gattacceca.

**Writing – original draft:** Alexis Courbet, Florence Gattacceca.

**Writing – review & editing:** Alexis Courbet, Florence Gattacceca.

## References

1. Gaspari A, Tyring S, Rosen T. Beyond a decade of 5% imiquimod topical therapy. *J Drugs Dermatol.* 2009; 8(5):467–74. PMID: [19537370](#)
2. Aspord C, Tramcourt L, Leloup C, Molens J-P, Leccia M-T, Charles J, et al. Imiquimod Inhibits Melanoma Development by Promoting pDC Cytotoxic Functions and Impeding Tumor Vascularization. *J Invest Dermatol.* 2014 Oct; 134(10):2551–61. <https://doi.org/10.1038/jid.2014.194> PMID: [24751730](#)
3. Moon S, Spencer J. Clearance of invasive melanoma with topical imiquimod. *J Drugs Dermatol.* 2013; 12(1):107–8. PMID: [23377337](#)
4. Green DS, Bodman-Smith MD, Dalglish a G, Fischer MD. Phase I/II study of topical imiquimod and intralesional interleukin-2 in the treatment of accessible metastases in malignant melanoma. *Br J Dermatol.* 2007 Feb; 156(2):337–45. <https://doi.org/10.1111/j.1365-2133.2006.07664.x> PMID: [17223875](#)
5. Florin V, Desmedt E, Vercambre-Darras S, Mortier L. Topical treatment of cutaneous metastases of malignant melanoma using combined imiquimod and 5-fluorouracil. *Invest New Drugs.* 2012 Aug; 30 (4):1641–5. <https://doi.org/10.1007/s10637-011-9717-2> PMID: [21748297](#)
6. Vacchelli E, Eggermont A, Sautès-Fridman C, Galon J, Zitvogel L, Kroemer G, et al. Toll-like receptor agonists for cancer therapy. *OncolImmunology.* 2013 Nov; 2(8):e25238. <https://doi.org/10.4161/onci.25238> PMID: [24083080](#)
7. Witt PL, Ritch PS, Reding D, McAuliffe TL, Westrick L, Grossberg SE, et al. Phase I trial of an oral immunomodulator and interferon inducer in cancer patients. *Cancer Res.* 1993 Nov 1; 53(21):5176–80. PMID: [8221654](#)
8. Cantisani C, Lazic T, Richetta A, Clerico R, Mattozzi C, Calvieri S. Imiquimod 5% cream use in dermatology, side effects and recent patents. *Recent Pat Inflamm Allergy Drug Discov.* 2012; 6(1):65–9. PMID: [22185454](#)
9. Deleuze-Masquéfa C, Gerebtzoff G, Subra G, Fabreguettes J-R, Ovens A, Carraz M, et al. Design and synthesis of novel imidazo[1,2-a]quinoxalines as PDE4 inhibitors. *Bioorg Med Chem.* 2004 Mar 1; 12 (5):1129–39. <https://doi.org/10.1016/j.bmc.2003.11.034> PMID: [14980625](#)
10. Deleuze-Masquéfa C., Moarbess G., Bonnet P., Pinguet F., Bazarbachi A. and Bressolle F. Imidazo[1,2-a]quinoxalines and derivatives thereof for treating cancers. International Patent PCT/EP2008/063290, 2009.
11. Moarbess G, Deleuze-Masquéfa C, Bonnard V, Gayraud-Paniagua S, Vidal J-R, Bressolle F, et al. In vitro and in vivo anti-tumoral activities of imidazo[1,2-a]quinoxaline, imidazo[1,5-a]quinoxaline, and pyrazolo[1,5-a]quinoxaline derivatives. *Bioorg Med Chem.* 2008 Jul 1; 16(13):6601–10. <https://doi.org/10.1016/j.bmc.2008.05.022> PMID: [18513976](#)
12. Moarbess G, El-Hajj H, Kfouri Y, El-Sabban ME, Lepelletier Y, Hermine O, et al. EAPB0203, a member of the imidazoquinoxaline family, inhibits growth and induces caspase-dependent apoptosis in T-cell lymphomas and HTLV-I-associated adult T-cell leukemia/lymphoma. *Blood.* 2008 Apr 1; 111(7):3770–7. <https://doi.org/10.1182/blood-2007-11-121913> PMID: [18218850](#)
13. Saliba J, Deleuze-Masquéfa C, Iskandarani A, El Eit R, Hmadi R, Mahon F-X, et al. EAPB0503, a novel imidazoquinoxaline derivative, inhibits growth and induces apoptosis in chronic myeloid leukemia cells. *Anticancer Drugs.* 2014 Jan 23; 7:1–9.
14. Savage P, Horton V, Moore J, Owens M, Witt P, Gore ME. A phase I clinical trial of imiquimod, an oral interferon inducer, administered daily. *Br J Cancer.* 1996; 74(9):1482–6. PMID: [8912549](#)

15. Lebbe C, Lorigan P, Ascierto P, Testori a, Bédane C, Middleton M, et al. Treatment patterns and outcomes among patients diagnosed with unresectable stage III or IV melanoma in Europe: a retrospective, longitudinal survey (MELODY study). *Eur J Cancer Oxf Engl* 1990. 2012 Nov; 48(17):3205–14.
16. Deleuze-Masquefa C, Moarbess G, Khier S, David N, Gayraud-Paniagua S, Bressolle F, et al. New imidazo[1,2-a]quinoxaline derivatives: synthesis and in vitro activity against human melanoma. *Eur J Med Chem.* 2009 Sep; 44(9):3406–11. <https://doi.org/10.1016/j.ejmech.2009.02.007> PMID: 19278757
17. Khier S, Moarbess G, Deleuze-Masquefa C, Solassol I, Margout D, Pinguet F, et al. Quantitation of imidazo[1,2- a] quinoxaline derivatives in human and rat plasma using LC/ESI-MS. *J Sep Sci.* 2009 May; 32(9):1363–73. <https://doi.org/10.1002/jssc.200800668> PMID: 19399864
18. Khier S, Gattaccea F, El Messaoudi S, Lafaille F, Deleuze-Masquefa C, Bompard J, et al. Metabolism and Pharmacokinetics of EAPB0203 and EAPB0503, Two Imidazoquinoxaline Compounds Previously Shown to Have Antitumoral Activity on Melanoma and T-Lymphomas. *Drug Metab Dispos.* 2010 Oct 1; 38(10):1836–47. <https://doi.org/10.1124/dmd.110.034579> PMID: 20660102
19. Burns EM, Yusuf N. Toll-Like Receptors and Skin Cancer. *Front Immunol [Internet].* 2014 Mar 31 [cited 2017 Apr 4]; 5. Available from: <http://journal.frontiersin.org/article/10.3389/fimmu.2014.00135/abstract>
20. Schön M., Schön M. Imiquimod: mode of action: Imiquimod: mode of action. *Br J Dermatol.* 2007 Dec 7; 157:8–13. <https://doi.org/10.1111/j.1365-2133.2007.08265.x> PMID: 18067624
21. Denning DP, Hirose T. Anti-tubulins DEPendably induce apoptosis. *Nat Cell Biol.* 2014 Aug 1; 16(8):741–3. <https://doi.org/10.1038/ncb3012> PMID: 25082198
22. Narayan R, Nguyen H, Bentow JJ, Moy L, Lee DK, Greger S, et al. Immunomodulation by imiquimod in patients with high-risk primary melanoma. *J Invest Dermatol.* 2012 Jan; 132(1):163–9. <https://doi.org/10.1038/jid.2011.247> PMID: 21850019
23. Morjaria S, Deleuze-Masquefa C, Lafont V, Gayraud S, Bompard J, Bonnet P a, et al. Impairment of TNF-alpha production and action by imidazo[1,2- alpha] quinoxalines, a derivative family which displays potential anti-inflammatory properties. *Int J Immunopathol Pharmacol.* 2006; 19(3):525–38. <https://doi.org/10.1177/039463200601900308> PMID: 17026837
24. Fang X, Shao L, Zhang H, Wang S. Web-based tools for mining the NCI databases for anticancer drug discovery. *J Chem Inf Comput Sci.* 2004; 44(1):249–57. <https://doi.org/10.1021/ci034209i> PMID: 14741034
25. Zghaib Z, Guichou JF, Vappiani J, Bec N, Hadj-Kaddour K, Vincent LA, et al. New imidazoquinoxaline derivatives: Synthesis, biological evaluation on melanoma, effect on tubulin polymerization and structure-activity relationships. *Bioorg Med Chem.* 2016; 24(11):2433–40. <https://doi.org/10.1016/j.bmc.2016.04.004> PMID: 27094151
26. Jordan MA, Thrower D, Wilson L. Effects of vinblastine, podophyllotoxin and nocodazole on mitotic spindles. Implications for the role of microtubule dynamics in mitosis. *J Cell Sci.* 1992 Jul; 102 (Pt 3):401–16.
27. Williams RJ, Lee J. Preparation of tubulin from brain. *Methods Enzymol.* 1982; 85 Pt B:376–85.
28. Bonfils C, Bec N, Lacroix B, Hurricane M-C, Larroque C. Kinetic analysis of tubulin assembly in the presence of the microtubule-associated protein TOGp. *J Biol Chem.* 2007 Feb 23; 282(8):5570–81. <https://doi.org/10.1074/jbc.M605641200> PMID: 17178729
29. Chou T-C. Drug combination studies and their synergy quantification using the Chou-Talalay method. *Cancer Res.* 2010 Jan 15; 70(2):440–6. <https://doi.org/10.1158/0008-5472.CAN-09-1947> PMID: 20068163
30. Chou T-C. Theoretical Basis, Experimental Design, and Computerized Simulation of Synergism and Antagonism in Drug Combination Studies. *Pharmacol Rev.* 2006; 58(3):621–81. <https://doi.org/10.1124/pr.58.3.10> PMID: 16968952
31. Trott O, Olson AJ. AutoDock Vina: improving the speed and accuracy of docking with a new scoring function, efficient optimization and multithreading. *J Comput Chem.* 2010; 31(2):455–61. <https://doi.org/10.1002/jcc.21334> PMID: 19499576
32. Sanner MF. Python: a programming language for software integration and development. *J Mol Graph Model.* 1999; 17(1):57–61. PMID: 10660911
33. Irwin JJ, Shoichet BK. ZINC—a free database of commercially available compounds for virtual screening. *J Chem Inf Model.* Jan; 45(1):177–82. <https://doi.org/10.1021/ci049714> PMID: 15667143
34. Morris GM, Goodsell DS, Halliday RS, Huey R, Hart WE, Belew RK, et al. Automated docking using a Lamarckian genetic algorithm and an empirical binding free energy function. *J Comput Chem.* 1998 Nov 15; 19(14):1639–62.
35. Bhattacharyya B, Wolff J. Promotion of fluorescence upon binding of colchicine to tubulin. *Proc Natl Acad Sci U S A.* 1974; 71(7):2627–31. PMID: 4527949

36. Zhang C, Yang N, Yang C-H, Ding H-S, Luo C, Zhang Y, et al. S9, a novel anticancer agent, exerts its anti-proliferative activity by interfering with both PI3K-Akt-mTOR signaling and microtubule cytoskeleton. *PloS One*. 2009 Jan; 4(3):e4881. <https://doi.org/10.1371/journal.pone.0004881> PMID: 19293927
37. Jordan M a. Mechanism of action of antitumor drugs that interact with microtubules and tubulin. *Curr Med Chem Anti-Cancer Agents*. 2002 Jan; 2(1):1–17. PMID: 12678749
38. Mollinedo F, Gajate C. Microtubules, microtubule-interfering agents and apoptosis. *Apoptosis*. 2003; 8 (5):413–50. PMID: 12975575
39. De Brabander M, Van de Veire R, Aerts F, Geuens S, Hoebeke J. A New Culture Model Facilitating Rapid Quantitative Testing of Mitotic Spindle Inhibition in Mammalian Cells. *J Natl Cancer Inst*. 1976; 56 (2):357–63. PMID: 1255766
40. Ravelli RBG, Gigant B, Curmi PA, Jourdain I, Lachkar S, Sobel A, et al. Insight into tubulin regulation from a complex with colchicine and a stathmin-like domain. *Nature*. 2004; 428(6979):198–202. <https://doi.org/10.1038/nature02393> PMID: 15014504
41. De Martino G, Edler MC, La Regina G, Coluccia A, Barbera MC, Barrow D, et al. New arylthioindoles: potent inhibitors of tubulin polymerization. 2. Structure-activity relationships and molecular modeling studies. *J Med Chem*. 2006; 49(3):947–54. <https://doi.org/10.1021/jm050809s> PMID: 16451061
42. Wang LG, Liu XM, Kreis W, Budman DR. The effect of antimicrotubule agents on signal transduction pathways of apoptosis: a review. *Cancer Chemother Pharmacol*. 1999 Jan; 44(5):355–61. <https://doi.org/10.1007/s002800050989> PMID: 10501907
43. Gundersen G, Cook T. Microtubules and signal transduction. *Curr Opin Cell Biol*. 1999; 11(1):81–94. PMID: 10047525
44. Jordan MA, Wilson L. Microtubules as a target for anticancer drugs. *Nat Rev Cancer*. 2004; 4(4):253–65. <https://doi.org/10.1038/nrc1317> PMID: 15057285
45. Giannakakou P, Sackett D, Fojo T. Tubulin/microtubules: still a promising target for new chemotherapeutic agents. *J Natl Cancer Inst*. 2000 Feb 2; 92(3):182–3. PMID: 10655426
46. Lu Y, Chen J, Xiao M, Li W, Miller DD. An Overview of Tubulin Inhibitors That Interact with the Colchicine Binding Site. *Pharm Res*. 2012 Nov; 29(11):2943–71. <https://doi.org/10.1007/s11095-012-0828-z> PMID: 22814904
47. Gajate C, Barasoain I, Andreu JM, Mollinedo F. Induction of apoptosis in leukemic cells by the reversible microtubule-disrupting agent 2-methoxy-5-(2',3',4'-trimethoxyphenyl)-2,4,6-cycloheptatrien-1-one: protection by Bcl-2 and Bcl-X(L) and cell cycle arrest. *Cancer Res*. 2000 May 15; 60(10):2651–9. PMID: 10825137
48. Prota AE, Danel F, Bachmann F, Bargsten K, Buey RM, Pohlmann J, et al. The novel microtubule-destabilizing drug BAL27862 binds to the colchicine site of tubulin with distinct effects on microtubule organization. *J Mol Biol*. 2014 Apr 17; 426(8):1848–60. <https://doi.org/10.1016/j.jmb.2014.02.005> PMID: 24530796
49. Massarotti A, Coluccia A, Silvestri R, Sorba G, Brancale A. The tubulin colchicine domain: a molecular modeling perspective. *ChemMedChem*. 2012 Jan 2; 7(1):33–42. <https://doi.org/10.1002/cmdc.201100361> PMID: 21990124
50. Weber A, Kirejczyk Z, Potthoff S, Ploner C, Häcker G. Endogenous Noxa Determines the Strong Proapoptotic Synergism of the BH3-Mimetic ABT-737 with Chemotherapeutic Agents in Human Melanoma Cells. *Transl Oncol*. 2009 Jun; 2(2):73–83. PMID: 19412422
51. Sidky YA, Borden EC, Weeks CE, Reiter MJ, Hatcher JF, Bryan GT. Inhibition of Murine Tumor Growth by an Interferon-inducing Imidazoquinolinamine. *Cancer Res*. 1992; 52:3528–33. PMID: 1377595
52. Hemmi H, Kaisho T, Takeuchi O, Sato S, Sanjo H, Hoshino K, et al. Small anti-viral compounds activate immune cells via the TLR7 MyD88-dependent signaling pathway. *Nat Immunol*. 2002 Feb; 3(2):196–200. <https://doi.org/10.1038/ni758> PMID: 11812998
53. Schön MP, Bong a. B, Drewniok C, Herz J, Geilen CC, Reifenberger J, et al. Tumor-Selective Induction of Apoptosis and the Small-Molecule Immune Response Modifier Imiquimod. *J Natl Cancer Inst*. 2003 Aug 5; 95(15):1138–49. PMID: 12902443
54. Schön MP, Wienrich BG, Drewniok C, Bong AB, Eberle J, Geilen CC, et al. Death receptor-independent apoptosis in malignant melanoma induced by the small-molecule immune response modifier imiquimod. *J Invest Dermatol*. 2004 May; 122(5):1266–76. <https://doi.org/10.1111/j.0022-202X.2004.22528.x> PMID: 15140231
55. Han J-H, Lee J, Jeon S-J, Choi E-S, Cho S-D, Kim B-Y, et al. In vitro and in vivo growth inhibition of prostate cancer by the small molecule imiquimod. *Int J Oncol*. 2013 Jun; 42(6):2087–93. <https://doi.org/10.3892/ijo.2013.1898> PMID: 23588478